

## NSLS-II BEAM DIAGNOSTICS OVERVIEW\*

O. Singh<sup>#</sup>, R. Alforque, B. Bacha, A. Blednykh, P. Cameron, W. Cheng, L.B. Dalesio, A.J. Della Penna, L. Doom, R. P. Fliller, G. Ganetis, R. Heese, H-C Hseuh, E.D. Johnson, B.N. Kosciuk, S.L. Kramer, S. Krinsky, J. Mead, S. Ozaki, D. Padrazo, I. Pinayev, V. Ravindranath, J. Rose, T. Shaftan, S. Sharma, J. Skaritka, T. Tanabe, Y. Tian, F.J. Willeke, L-H Yu, NSLS-II, BNL, Upton, New York 11973-5000 U.S.A.

### Abstract

A new 3rd generation light source (NSLS-II) is in the early stages of construction at Brookhaven National Laboratory. The NSLS-II facility will provide ultra high brightness and flux with exceptional beam stability. It presents several challenges for diagnostics and instrumentation, related to the extremely small emittance. In this paper, we present an overview of all planned instrumentation systems, results from research and development activities; and then focus on other challenging aspects.

### INTRODUCTION

The NSLS-II project will be a state-of-the-art synchrotron radiation facility [1-6] featuring ultra-high photon brightness with extremely low emittance. It will consist of a 200 MeV S-band linac, 0.2–3 GeV ramping booster, transport lines, and 3 GeV storage ring with the latest available beam instrumentation and diagnostics systems. Table 1 lists storage ring (SR) and booster parameters relevant to the electron beam diagnostics.

Table 1: SR and Booster Parameters for Diagnostics

| Parameter                           | SR           | Booster     |
|-------------------------------------|--------------|-------------|
| Energy (GeV)                        | 3.0          | 0.2 – 3     |
| RF frequency (MHz)                  | 499.68       | 499.68      |
| Harmonic number                     | 1320         | 264         |
| Circumference (m)                   | 792          | 158.4       |
| Revolution period, $T_0$ ( $\mu$ s) | 2.642        | 0.528       |
| Number of bunches                   | 1–1056       | 1–150       |
| Repetition rate (Hz)                | -            | 1           |
| Max. average current (mA)           | 500          | 28          |
| Max. single bunch current (mA)      | 2–5          | 1           |
| Bunch length ( $\sigma$ ps)         | 15-30        | 15          |
| Tunes - $Q_x, Q_y$                  | 33.36, 16.28 | 10.91, 6.69 |
| Horizontal Emittance (nm-rad)       | 0.5-2        | 50          |
| Synchrotron freq., $f_s$ (kHz)      | 3.0-3.6      | 22          |

The storage ring has 1,320 buckets with ~20% of the buckets left empty to alleviate ion trapping the stored electron beam. The average design current is 500 mA, with ~ 1000 bunches. Other fill patterns, such as camshaft, will also be explored, with single-bunch current limited to 2-5 mA. The 3<sup>rd</sup> harmonic RF cavities will be used to lengthen the bunches from ~15ps to ~30 ps, to

assure top-off injection frequency no more than 1/minute to maintain 1% beam current stability.

To realize the benefits of the high brightness and small sizes of the NSLS-II sources, photon beams must be exceedingly stable both in position and angle, to the level of better than 10% of beam sizes and divergence. The most stringent beam measurement and stability requirement will be for the vertical position at the short ID source ( $\sigma_y=3.1 \mu$ m); this will require special consideration for measuring both electron and photon beams.

### INJECTOR DIAGNOSTICS

The injector beam diagnostics goals are to: 1) provide smooth commissioning, 2) support wide dynamic intensity range in a single-bunch and multi-bunch operation, and 3) provide stable beam for top-up injection while maintaining small emittance.

The injector linac [1] will consist of a 100kV electron gun with grid modulation at 500 MHz, sub-harmonic prebuncher, 3 GHz prebuncher/ buncher, and accelerator tanks. It will be capable of operating in single-bunch or multi-bunch (40-150) mode. Some linac parameters for diagnostics are listed in Table 2.

Table 2: Linac Parameters for Diagnostics

| Linac Parameter             | Nominal Value        |
|-----------------------------|----------------------|
| Energy                      | 200 MeV              |
| Emittance                   | 55 mm-mrad           |
| Energy spread, single bunch | $\pm 0.5\%$          |
| Energy spread, multi bunch  | $\pm 1\%$            |
| Bunch train length          | 40–150 bunches, 2 ns |
| Bunch charge, single bunch  | 10 pC–0.5 nC         |
| Bunch charge, multi bunch   | < 15 nC              |

The wall current and fast current monitors, deployed at strategic locations, will provide bunch longitudinal profile in single- and multi-bunch operation, needed for injector tuning. The interface requirements for these current monitors are being evaluated for the control interface system. The integrating transformer and DC current transformer [7] will provide beam charge and current information for non-destructive measurements. Some of these transformer signals will also be interfaced to the beam containment system to secure the safety envelope. An array of fluorescent screens [8] is deployed to provide transverse profiles at strategic locations throughout the injector. The energy slits are used to control energy spread. Table 3 provides a list of injector diagnostics. The

\*Work supported by the U.S. DOE under contract No. DE-AC02-98CH10886

<sup>#</sup>singh@bnl.gov

linac and transport lines' RF BPMs will be single-pass BPMs; the booster RF BPMs will be both single-pass and multi-turn BPMs.

Table 3 : List of Injector Diagnostics

| Monitor              | Injector |     |         |     |
|----------------------|----------|-----|---------|-----|
|                      | Linac    | LTB | Booster | BTS |
| Wall Current Monitor | 5        |     |         |     |
| Fast CT              |          | 2   | 1       | 2   |
| Integrating CT       |          | 2   |         | 2   |
| DC CT                |          |     | 1       |     |
| Fluorescent Screen   | 3        | 9   | 6       | 9   |
| Energy Slit          |          | 1   |         | 1   |
| Beam Dumps           |          | 2   |         | 1   |
| RF BPM               | 3        | 6   | 24      | 7   |

CT = current transformer    BPM = beam position monitor

A visible light beamline is also planned for the booster, to provide bunch profile and bunch length measurements. A tune monitor will also be installed in the booster.

### STORAGE RING DIAGNOSTICS

The beam diagnostic systems are designed to provide a complete characterization of the beam properties including beam closed orbit, size, tune, circulating current, fill pattern, lifetime, chromaticity, beam loss pattern, beam density distribution, emittance, and bunch length [9]. A large number of beam monitors and beam drivers will be installed in the storage ring. Synchrotron radiation beamlines are also planned.

#### Beam Position Monitors

The layout of the BPMs and magnets in one cell is shown in Fig. 1.

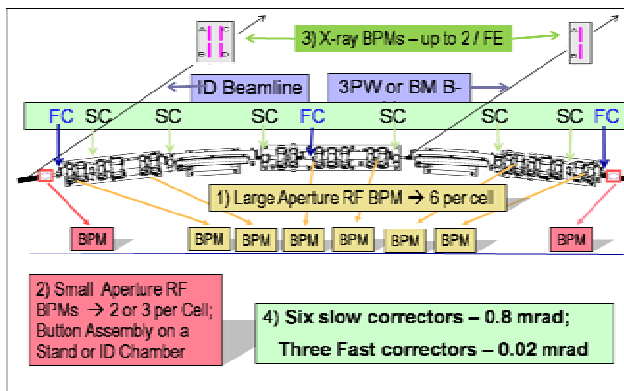


Figure 1: BPMs and magnets in a storage ring cell.

Each cell will have six large-aperture (25mm) RF BPMs mounted on elliptical chambers, up to three small-aperture (10mm) RF BPMs located in the ID straight section, and up to two photon BPMs in each beamline. The number of RF and photon BPMs will be determined by the type of beamline. For example, a canted beamline will require three small-aperture RF BPMs.

Due to stringent orbit measurement and stability requirements, a significant effort has been invested in the NSLS-II project to achieve the highest level of electron orbit measurement resolution and stability. The effort can be divided into four critical technical areas, each impacting the overall RF BPM performance: a) RF button geometry, b) RF button mechanical mounting stability, c) Vacuum chamber microwave modes, and d) RF BPM electronics.

*RF Button Geometry* - The sensitivity of large-aperture RF buttons was first optimized by reducing the horizontal separation from 32 mm to 16 mm [10]. The mechanical constraints of this comparatively close horizontal spacing resulted in the two buttons in one flange design. With the overall geometry defined, button internal dimensions were optimized via GdfidL simulations to minimize distortion due to trapped mode heating [11-14]. This resulted in a button diameter of 7 mm, thickness of 2 mm, and spacing to the outer housing of 0.25 mm. Fig. 2 shows the new button design with one flange mounted on the top.

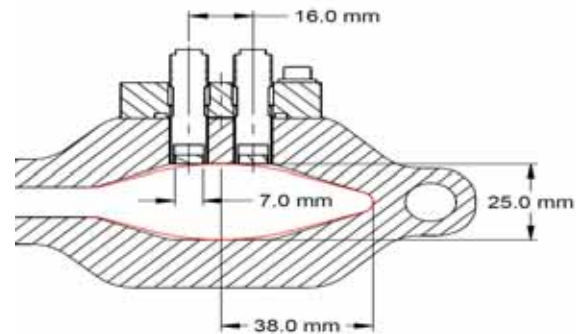


Figure 2: A new button design with two buttons in a single flange for large-aperture RF BPMs mounted on the top. A similar flange with two buttons is mounted at the bottom (not shown).

The two-in-one 4mm RF buttons separated by 9.6 mm is planned for use with small-aperture RF BPMs. Table 4 lists the geometry and sensitivities for large- and small-aperture RF BPMs. Note that y sensitivity for small-aperture RF BPMs is 0.15 /mm when x-separation is 9.6 mm and it increases to 0.26 /mm when button flange is rotated to get an effective x-separation at 4 mm.

Table 4: Geometry and Sensitivities for Large- and Small-Aperture RF BPMs for NSLS-II

| RF Button            | Large-Aperture | Small Aperture |
|----------------------|----------------|----------------|
| Button diameter (mm) | 7              | 4              |
| x- Separation (mm)   | 16             | 4-9.6          |
| y- Separation (mm)   | 25             | 10             |
| x-Sensitivity (/mm)  | 0.1            | 0.15-0.27      |
| y-Sensitivity (/mm)  | 0.1            | 0.26-0.15      |

*RF Buttons' Mechanical Mounting Stability* - The large-aperture RF BPM button assemblies are mounted on the multiple vacuum chamber. A invar support plate,

mounted rigidly on the magnet girder, is fastened to the vacuum chamber near the button assembly. This invar plate restricts x/y thermal motion to be less than 500nm and 200nm respectively; and sufficient flexibility in the z direction to accommodate chamber expansion due to varying thermal conditions [1].

The small-aperture RF BPM button assemblies will be mounted on a high-stability support being developed at NSLS-II [15]. The design utilizes invar alloy for the primary structural element and consists of an array of four 50mm-diameter rods bolted to a base plate. The goal is to limit vertical thermal expansion to <100 nm per 8-hr period. Fig. 3 shows the result of a transient thermal finite element analysis performed on this design using free convection heat transfer applied to all exposed surfaces with a temperature of  $25.0 \pm 0.1^\circ\text{C}$  per hour. The floor temperature boundary condition was set to  $25.0 \pm 0.1^\circ\text{C}$  per 24-hour period. The result of this is roughly  $\pm 60$  nm of thermal deformation in the vertical direction over a 24-hr interval, meeting the required  $\pm 100$  nm specification.

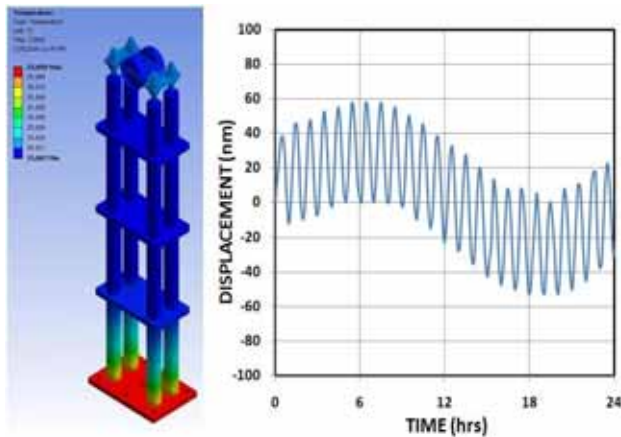


Figure 3: Temperature distribution and plot of vertical deformation of 1.2m stand.

*Vacuum chamber microwave modes* - The multipole vacuum chambers have small height in the area between the oval beam chamber and the antechamber (Fig. 4).



Figure 4: NSLS-II Multipole vacuum chamber.

This structure behaves like a ridge waveguide and the cut-off frequency of this waveguide mode ( $H_{10}$ -mode) is 445.8 MHz. This frequency falls below BPM electronic receiver frequency (500 MHz) which could result in bad BPM reading. To verify this effect, the resonance and quality factors were measured for a 3.4m-long prototype multipole vacuum chamber (Table 5). Note that in first 6

mode frequency listed, BPM receiver frequency falls in between 4<sup>th</sup> and 5<sup>th</sup> mode. We wish to damp all Higher Order Modes (HOMs) in the structure. The solution to this problem is in the early stages of development; we are exploring either an RF shunt or magnetic loops implementation.

Table 5 : Measured Resonance and Quality Factors\*

| f (MHz) | Q <sub>0</sub> | Computed | f (MHz) | Q <sub>0</sub> | Computed |
|---------|----------------|----------|---------|----------------|----------|
| 447.05  | 4100           | 447.42   | 490.48  | 3500           | 478.87   |
| 457.58  | 3800           | 453.88   | 511.30  | 3400           | 496.78   |
| 472.14  | 3700           | 464.45   | 535.16  | 3100           | 517.83   |

\*Note: The 500MHz BPM frequency lies between resonance modes.

*RF BPM Electronics* - The commercially available digital BPM receiver (Liberia Brilliance from Instrument technology) is being evaluated under laboratory as well as under beam conditions; and results show that it meets or exceeds the technical NSLS-II requirements [9]. However, a few questions relating to maintenance issues and possible obsolescence are being addressed with the vendor. For example, the FPGA device used in the current Brilliance is no longer supported by the most recent software development tools provided by the FPGA vendor. This will make modifications to the FPGA firmware more difficult as the years progress and this issue need to be addressed.

A comparison of RF BPM electronics under APS beam conditions was done recently, employing 1) APS in-house FPGA BPMs, 2) Brilliance BPMs; and 3) MXBPMs from Bergoz, Inc. The beam motion spectrum comparison measured with turn-by-turn data from APS and Brilliance BPMs shows excellent agreement under stored beam conditions as well as transient conditions during top-up pulse [16]. Fig. 5 shows horizontal data from APS and Brilliance BPMs, caused by injection kickers.

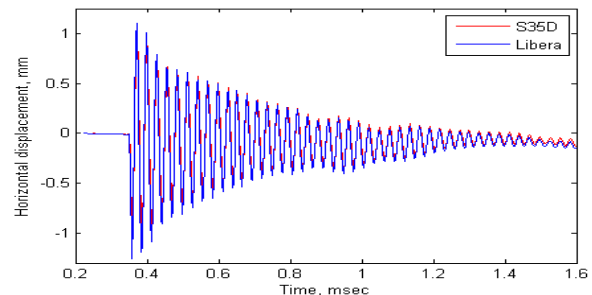


Figure 5: Horizontal transient caused by injection kickers. There is remarkable agreement in the two curves, with only a small offset observed toward the end of the transient.

The intensity and fill pattern dependence tests were done for the Brilliance unit, where a button signal from a stored beam was split into four and then applied to the BPM electronics. The intensity variation effect was created by 1) steering the beam by several mm; 2) fill pattern change effects were created by first filling 324

bunches uniformly; and 3) 15% and 30% holes were created by using a mis-matched injection bump. Fig. 6 shows that the noise levels for both x and y are < 20 nm with a 3-fold intensity change (from 9 a.u. to 3 a.u.). This level of performance exceeds the NSLS-II stability requirements.

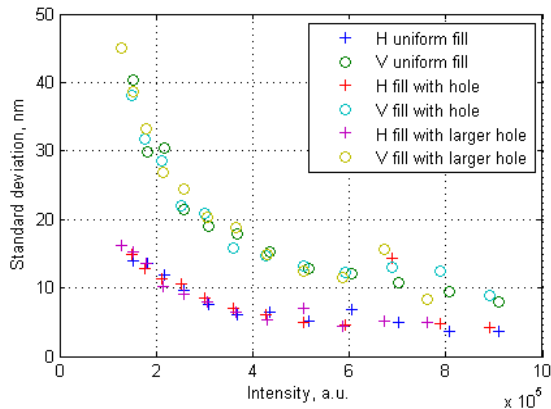


Figure 6: Beam position measurement noise dependence on intensity for different fills.

### Transverse Feedback

The NSLS-II storage ring is expected to exhibit transverse instabilities with a threshold current of 15mA [17]. The main instability sources include: the resistive wall impedance from small-gap vacuum chambers; ion trapping and fast-ion instability within long bunch train; and HOM impedance from discontinuity of vacuum chambers. To cure instabilities, an active transverse bunch-by-bunch feedback system will be required. A preliminary design is in progress. Fig. 7 shows a block diagram of a feedback system, consisting of 1) a button type BPM detector, 2) RF analog front end electronics, 3) digital processor, and 4) a stripline kicker.

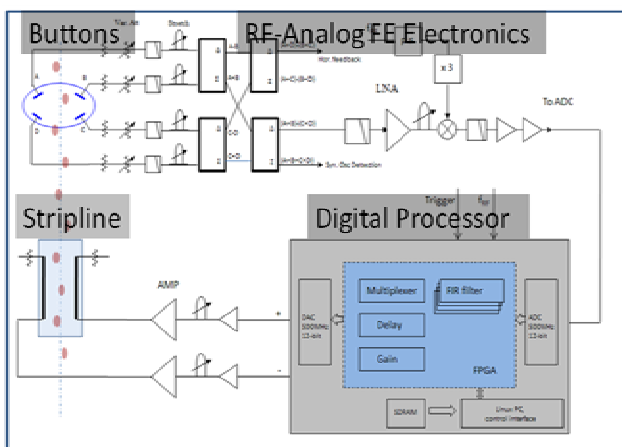


Figure 7 : A block diagram for a transverse bunch-to-bunch feedback system.

The FPGA-based digitizer will be used as the core of a feedback loop. The digital FIR filters will pass through the betatron oscillation frequency while blocking the DC and revolution harmonics; digital delay and phase can be

### Instrumentation

#### T03 - Beam Diagnostics and Instrumentation

adjusted in the processor as well. The precision delay adjustment will be done using coaxial line stretcher. The high shunt impedance and small beam impedance are desired for the stripline kicker as an actuator. Design work on a stripline kicker has begun.

### Photon Diagnostics

*X-ray pin-hole camera beamline* - The storage ring will provide extremely bright radiation sources characterized by extra-small transverse dimensions of the circulating electron beam. The beam dimensions will be monitored with a pinhole camera [18]. The plan is to develop an in-vacuum pin-hole located 3 m from the source and it is expected to provide vertical measurement resolution of 5 microns, which is adequate to measure a beam size of 12 microns. The first element of the pinhole beamline is a molybdenum filter/attenuator, as shown in Fig. 8.

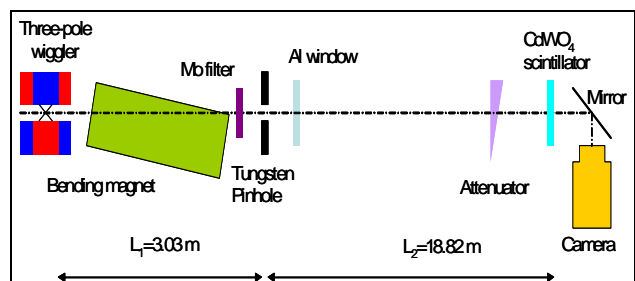


Figure 8 : Diagram of a pin-hole camera beamline.

It constitutes a foil, mounted inside of a crotch absorber in order to remove low-energy photons. The purpose is to reduce the heat load on downstream elements to an acceptable level and to improve resolution. Molybdenum was chosen for its high melting temperature and high heat conduction. The thickness of the foil represents a compromise between temperature rise of the foil (which is cooled by conduction) and sufficient flux of the X-ray photons. The filter is followed by a fixed tungsten pinhole, also mounted on the crotch absorber.

*Visible light monitor beamline* - Figure 9 shows a visible synchrotron diagnostic beamline that will be built to measure various beam parameters. The source point is expected to be near the beginning of the second bending magnet in the cell, where x/y opening angles are 3 and 7 mrad, respectively.

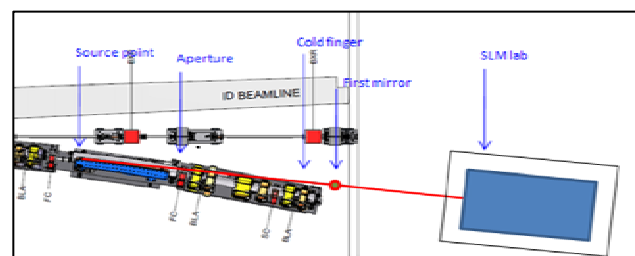


Figure 9: Diagram of a visible light monitor beamline.

The beamline is expected to use 500nm green light for streak camera measurements and other applications. The resolution is expected to be about 60 $\mu$ m, which makes the horizontal beam size measurement possible even at this wavelength. A double-sweep streak camera will be used to measure the longitudinal beam dynamics. Its versatility and high sensitivity make it an excellent choice for monitoring the bunch length with high resolution and for studying beam instabilities. The synchro-scan feature provides low-phase jitter for synchronous summing of signals and tracking phase dynamics. We are considering using either the Optronis model SC-10 or the Hamamatsu C5680 streak camera.

*Photon beam position monitors* - Photon beam position monitors made by FMB-Berlin are being considered for monitoring radiation from the insertion and bending magnet devices [19]. The Decker distortion [20] for removing background radiations will be evaluated for NSLS-II storage ring parameters. The blades will be designed and optimized to suit the requirements of NSLS-II. The photon BPM assembly will be mounted on a stable post and its location (elevation and transverse position) will be adjusted with 2D translation stages. The information obtained on the position of the photon beam will be incorporated into the orbit feedback system to provide the beam stability required for user applications. Similar devices at APS have been instrumental in achieving a high level of pointing stability of the photon beam [21].

### *Other Diagnostics*

Two sets of scrapers are planned, to provide several functions: 1) control the loss point for beam aborts or dumps, 2) limit the lifetime losses that create radiation on undulator magnets, and 3) for diagnostics and physics studies of the dynamic and momentum aperture of the ring [22]. The beam loss system will employ Cerenkov beam loss monitors, which will be located close to the vacuum chamber [23]. These units will be distributed, to capture as much of the beam particle loss as possible.

Several other diagnostics systems are also in a mature stage but are not discussed here. These systems include DC current measurement, fill pattern monitors, tune monitor, beam spectrum monitor, top-up current monitors and 3-position fluorescent screen. A bunch cleaner system is also planned.

## CONCLUSION

We have presented an overview of the proposed NSLS-II injector and storage ring diagnostics system. The results from research and development and preliminary design work have been discussed. The design level of subsystems is now mature and provides a firm basis to meet challenging requirements of diagnostics relating to the extremely small emittance.

## REFERENCES

- [1] NSLS-II Preliminary Design Report (PDR), <http://www.bnl.gov/nsls2/project/PDR/>.
- [2] S. Ozaki, et al., "Philosophy for NSLS-II Design with Sub-Nanometer Horizontal Emittance," Proc. of PAC07.
- [3] S. Krinsky, "Accelerator Physics Challenges for the NSLS-II Project," Proc. of PAC09.
- [4] J. Rose, et al., "Design consideration of the NSLS-II Injection Linac," Proc. of PAC07
- [5] T. Shaftan, et al., "Conceptual design of the NSLS-II Injection," Proc. of PAC07.
- [6] R. Fliller, et al., "Beam Transport and Diagnostics for the NSLS-II Injection System," Proc. Of PAC09.
- [7] <http://www.bergoz.com>
- [8] <http://www.radiabeam.com>
- [9] O. Singh, I. Pinayev, "Overview of Beam Instrumentation and Diagnostics for the NSLS-II Project," Proc. of BIW2008.
- [10] I. Pinayev, O. Singh, "Research & Development program on Beam position Monitors for NSLS-II Project," Proc. of EPAC08.
- [11] P. Cameron et al., "BPM Button Optimization to Minimize Distortion Due to Trapped Mode Heating," Proc. of PAC09.
- [12] P. Cameron et al., "Comparative Study of Button BPM Trapped Mode Heating," Proc. of PAC09.
- [13] P. Cameron et al., "Results from a Test Fixture for Button BPM Trapped Mode Measurements," Proc. of PAC09.
- [14] I. Pinayev, A. Blednykh, "Evaluation of Heat Dissipation in the BPM Buttons," Proc. of PAC09.
- [15] B. Kosciuk et al., "Development of High Stability Supports for NSLS-II RF BPMs," Proc. of PAC09.
- [16] I. Pinayev, O. Singh, NSLS-II, BNL; and G. Decker, APS, ANL, "Comparison of RF BPM Receivers for NSLS-II Project," Proc. of PAC09.
- [17] W. Cheng, "Design of Transverse Instability Feedback System," Internal Tech note, NSLS-II project.
- [18] I. Pinayev, B. Kosciuk and O. Singh, "Preliminary Design of Pinhole Cameras for NSLS-II Project," Proc. of PAC09.
- [19] <http://www.fmb-oxford.com>
- [20] G. Decker, O. Singh, Phys. Rev. ST Accel. Beams, 2, 112801 (1999).
- [21] G. Decker, O. Singh, "Beam Stability at the Advanced Photon Source," Proc. of PAC05.
- [22] S. Kramer, "Scrapers for the NSLS-II Storage Ring," Internal Tech note, NSLS-II project.
- [23] S. Kramer, "Injection beam loss monitor for NSLS-II Radiation protection," Internal Tech note, NSLS-II project.